Article

Changing patterns of global nitrogen deposition driven by socio-economic development

Jianxing Zhu [1,11], Yanlong Jia[2,11], Guirui Yu [1,3] ✉, Qiufeng Wang[1,3], Nianpeng He [4], Zhi Chen[1,3], Honglin He [1,3], Xianjin Zhu[5], Pan Li[6], Fusuo Zhang [7], Xuejun Liu [7], Keith Goulding [8], David Fowler[9] & Peter Vitousek [10]

Advances in manufacturing and trade have reshaped global nitrogen deposition patterns, yet their dynamics and drivers remain unclear. Here, we compile a comprehensive global nitrogen deposition database spanning 1977–2021, aggregating 52,671 site-years of data from observation networks and published articles. This database show that global nitrogen deposition to land is 92.7 Tg N in 2020. Total nitrogen deposition increases initially, stabilizing after peaking in 2015. Developing countries at low and middle latitudes emerge as new hotspots. The gross domestic product per capita is found to be highly and non-linearly correlated with global nitrogen deposition dynamic evolution, and reduced nitrogen deposition peaks higher and earlier than oxidized nitrogen deposition. Our findings underscore the need for policies that align agricultural and industrial progress to facilitate the peak shift or reduction of nitrogen deposition in developing countries and to strengthen measures to address NH_3 emission hotspots in developed countries.

Intense human activity has significantly altered Earth's nitrogen (N) cycle. Global emissions of reactive nitrogen (Nr) were estimated to be approximately 164 Tg in 1997 and 210 Tg in 2017[1]. Sources of atmospheric Nr are dominated by ammonia (NH_3) mainly from agricultural production, and N oxides from fossil fuel combustion[2]. After chemical transformation and physical transport in the atmosphere, NH_3 and NO_x are removed by wet and dry deposition (F_{Wet}, F_{Dry})[2,3]. N deposition can promote plant growth, crop yields and ecosystem carbon sinks[4,5]. However, excessive N input causes soil and water acidification[6],

reduces soil buffering capacity[7], decreases plant diversity[8] and threatens human health[9].

With the rapid development of industry, agriculture and urbanization, North America, Europe and East Asia became hotspots of global N deposition[3,10,11]. However, N deposition flux (F_N) in developed countries [defined by the World Bank as those with a gross national income per capita above 14,005 United States Dollar ($)] or developed regions (which include groups of developed countries), including the United States and Europe, has decreased substantially[12,13], and F_N in

[1]Key Laboratory of Ecosystem Network Observation and Modeling, Institute of Geographic Sciences and Natural Resources Research, Chinese Academy of Sciences, Beijing, China. [2]College of Forestry, Hebei Agricultural University, Baoding, China. [3]College of Resources and Environment, University of Chinese Academy of Sciences, Beijing, China. [4]Institute of Carbon Neutrality, Northeast Forestry University, Harbin, China. [5]College of Agronomy, Shenyang Agricultural University, Shenyang, China. [6]Institute of Surface-Earth System Science, School of Earth System Science, Tianjin University, Tianjin, China. [7]State Key Laboratory of Nutrient Use and Management, College of Resources and Environmental Sciences, National Academy of Agriculture Green Development, China Agricultural University, Beijing, China. [8]Sustainable Agricultural Sciences Department, Rothamsted Research, Harpenden, UK. [9]Centre for Ecology and Hydrology, Penicuik, UK. [10]Department of Biology, Stanford University, Stanford, USA. [11]These authors contributed equally: Jianxing Zhu, Yanlong Jia. ✉e-mail: yugr@igsnrr.ac.cn

China has stabilized or declined recently because of better environmental governance and economic structural transformation[14,15]. The predicted global population increase, high demand for food and energy, industrial relocation and rapid trade development[1,16] are likely to change patterns of F_N. However, deposition observation networks are predominantly located in the United States, Europe and East Asia[12–15]. Few observation sites exist in developing countries (those with a gross national income per capita below $14,005) and developing regions (groups of developing countries), and substantial gaps in records exist in Latin America and Africa[17]. Systematic reviews of global N deposition monitoring data are limited, and models of global N deposition have modest spatial resolution and are based primarily on highly uncertain emission inventories[18].

Nr emission (E_{Nr}) distribution, the intensity of agricultural and industrial activity and climate are key factors affecting the spatiotemporal patterns of F_N[15]. E_{Nr} and agricultural N pollution are closely related to socioeconomic development, such as gross domestic product per capita (GDPpc)[19,20]. Attempts to reconcile economic development and environmental governance have led to the introduction of better N management and technologies, and the relocation of industries[1]. However, compared with developed countries, developing countries lag behind in terms of N use efficiency, N management and the widespread use of emission reduction technologies[20]. It is important to clarify how socioeconomic development drives the dynamic evolution and changing global patterns of F_N in developing countries, which has significant implications for realizing the goal of halve nitrogen waste, as outlined in the Colombo Declaration[21].

In this work, we compile data from international N deposition networks and 1390 published papers and construct a Monitoring-based Global Nitrogen Deposition (MGND) database for 1977–2021, encompassing more than 50,000 site-years of data (Supplementary Table 1 and Supplementary fig. 1). Based on the cascading network of GDPpc → E_{Nr} → satellite N column concentration (C_N, e.g., NH_3 or NO_2) → meteorological factors (e.g., mean annual precipitation, MAP) → F_N, which represents the driving mechanism and qualitative relationship of global N deposition, we develop a framework to generate a global N deposition grid dataset

with a resolution of 0.125° × 0.125° for 2008–2020. We reveal the pattern and dynamic evolution of global N deposition, explore the mechanisms driving N deposition, including socioeconomic development, and propose measures for better N management in developing countries.

Results and discussion
Status of global N deposition in 2020
The global average total N deposition flux (F_{Tot}) to land areas in 2020 was 7.0 kg N ha^{-1} yr^{-1}, of which ammonium (F_{NHx}) and nitrate (F_{NOy}) contributed 4.3 and 2.7 kg N ha^{-1} yr^{-1}, respectively (Table 1). The global annual input of N through deposition to land in 2020 was approximately 92.7 Tg N, equivalent to 84% of the global agricultural N fertilizer use in that year (110.5 Tg N)[22], and lower than global estimate of E_{Nr} (125.7–179.5 Tg N, Supplementary Table 2). Our estimate is comparable to the simulation results of multiple atmospheric chemical transport models (90.4 Tg N yr^{-1} to global land in 2010[23]) and measurement–model fusion work (87.2 Tg N yr^{-1} to global land in 2010[24]), and higher than that from results evaluated from the history of anthropogenic N inputs (63.9 Tg N yr^{-1} to global land in 2010s[25]).

The current spatial pattern of global N deposition is high in middle and low latitudes (30 °S–30 °N) and low in high latitudes (>50°N and 50°S) (Fig. 1a). F_N in South Asia, East Asia, Southeast Asia, and South America is higher than that in Western Europe and North America (Table 1). Especially high levels of F_N are concentrated in northern India, north China, and eastern China, with values of 40–60 kg N ha^{-1} yr^{-1}. The spatial distribution patterns of F_{NHx}, F_{NOy}, F_{Dry} and F_{Wet} are the same as those of F_{Tot} (Supplementary Fig. 2). A surprisingly high level of F_{NHx} with value of 4.5 kg N ha^{-1} yr^{-1} is also found in Africa, which is far higher than previous results[23,26]. Further analysis shows that C_{NH3} in Africa is almost comparable with that in North America, East Asia, and Western Europe in recent years (Supplementary Fig. 3), consistent with previous research[27]. The total amount of NH_3 emissions (E_{NH3}) from the emission inventory of Community Emission Data System (CEDS)[28] in Africa is also higher than that in North America and Western Europe. This suggests that previous studies may have greatly underestimated N deposition in Africa.

Table 1 | Regional atmospheric N deposition flux and total input in 2020

Regions	F_{Dry} (kg N ha^{-1} yr^{-1})			F_{Wet} (kg N ha^{-1} yr^{-1})			F_{Tot} (kg N ha^{-1} yr^{-1})			N inputs (Tg N yr^{-1})
	NHx	NOy	NHx+NOy	NHx	NOy	NHx+NOy	NHx	NOy	NHx+NOy	NHx+NOy
Africa	2.79 ± 0.54	1.42 ± 0.18	4.21 ± 0.58	1.65 ± 0.05	1.19 ± 0.12	2.84 ± 0.17	4.45 ± 0.52	2.61 ± 0.30	7.05 ± 0.59	21.02 ± 1.76
Central America	3.30 ± 0.66	2.00 ± 0.33	5.3 ± 0.93	2.36 ± 0.11	1.72 ± 0.15	4.08 ± 0.24	5.65 ± 0.71	3.73 ± 0.41	9.38 ± 1.01	2.47 ± 0.27
Central Asia	1.49 ± 0.33	1.07 ± 0.09	2.56 ± 0.42	1.10 ± 0.31	0.78 ± 0.17	1.88 ± 0.48	2.59 ± 0.64	1.85 ± 0.25	4.44 ± 0.89	1.77 ± 0.36
East Asia	3.56 ± 0.09	2.22 ± 0.01	5.78 ± 0.09	3.19 ± 0.05	2.60 ± 0.11	5.79 ± 0.15	6.75 ± 0.08	4.82 ± 0.10	11.57 ± 0.17	13.33 ± 0.19
East Europe	0.63 ± 0.08	0.44 ± 0.04	1.07 ± 0.04	0.70 ± 0.07	0.54 ± 0.07	1.24 ± 0.15	1.33 ± 0.06	0.98 ± 0.11	2.31 ± 0.12	4.02 ± 0.21
Greenland	0.14 ± 0.08	0.05 ± 0.01	0.20 ± 0.09	0.06 ± 0.01	0.05 ± 0.004	0.11 ± 0.01	0.20 ± 0.06	0.10 ± 0.01	0.30 ± 0.08	0.06 ± 0.02
North America	1.44 ± 0.06	0.70 ± 0.03	2.13 ± 0.09	1.06 ± 0.04	0.75 ± 0.03	1.81 ± 0.06	2.5 ± 0.02	1.44 ± 0.05	3.94 ± 0.07	7.45 ± 0.13
Oceania	1.72 ± 0.70	0.73 ± 0.19	2.45 ± 0.75	0.95 ± 0.24	0.69 ± 0.16	1.64 ± 0.41	2.67 ± 0.85	1.42 ± 0.35	4.09 ± 1.06	3.41 ± 0.89
South America	3.52 ± 0.66	1.78 ± 0.34	5.30 ± 0.90	2.29 ± 0.19	1.66 ± 0.24	3.95 ± 0.38	5.82 ± 0.83	3.44 ± 0.57	9.25 ± 1.28	16.29 ± 2.25
South Asia	8.41 ± 0.48	4.14 ± 0.58	12.55 ± 0.83	5.17 ± 0.25	4.18 ± 0.28	9.34 ± 0.47	13.57 ± 0.23	8.32 ± 0.80	21.89 ± 0.84	9.40 ± 0.36
Southeast Asia	3.60 ± 0.32	2.38 ± 0.24	5.98 ± 0.52	3.61 ± 0.02	2.54 ± 0.20	6.15 ± 0.18	7.21 ± 0.34	4.92 ± 0.21	12.12 ± 0.37	5.18 ± 0.16
West Asia	1.46 ± 0.20	1.88 ± 0.24	3.35 ± 0.43	1.47 ± 0.29	1.08 ± 0.15	2.55 ± 0.45	2.93 ± 0.48	2.96 ± 0.37	5.89 ± 0.84	3.97 ± 0.56
West Europe	2.31 ± 0.24	1.39 ± 0.08	3.70 ± 0.31	2.68 ± 0.08	2.03 ± 0.02	4.71 ± 0.10	4.99 ± 0.32	3.42 ± 0.10	8.41 ± 0.41	4.31 ± 0.21
Global	2.46 ± 0.28	1.39 ± 0.13	3.85 ± 0.37	1.80 ± 0.05	1.35 ± 0.08	3.15 ± 0.12	4.27 ± 0.33	2.73 ± 0.21	7.00 ± 0.48	92.68 ± 6.39

The values are Mean ± SD among the three random forest models' results. F_{Wet}, F_{Dry}, and F_{Tot} are wet, dry, and total N deposition, respectively.

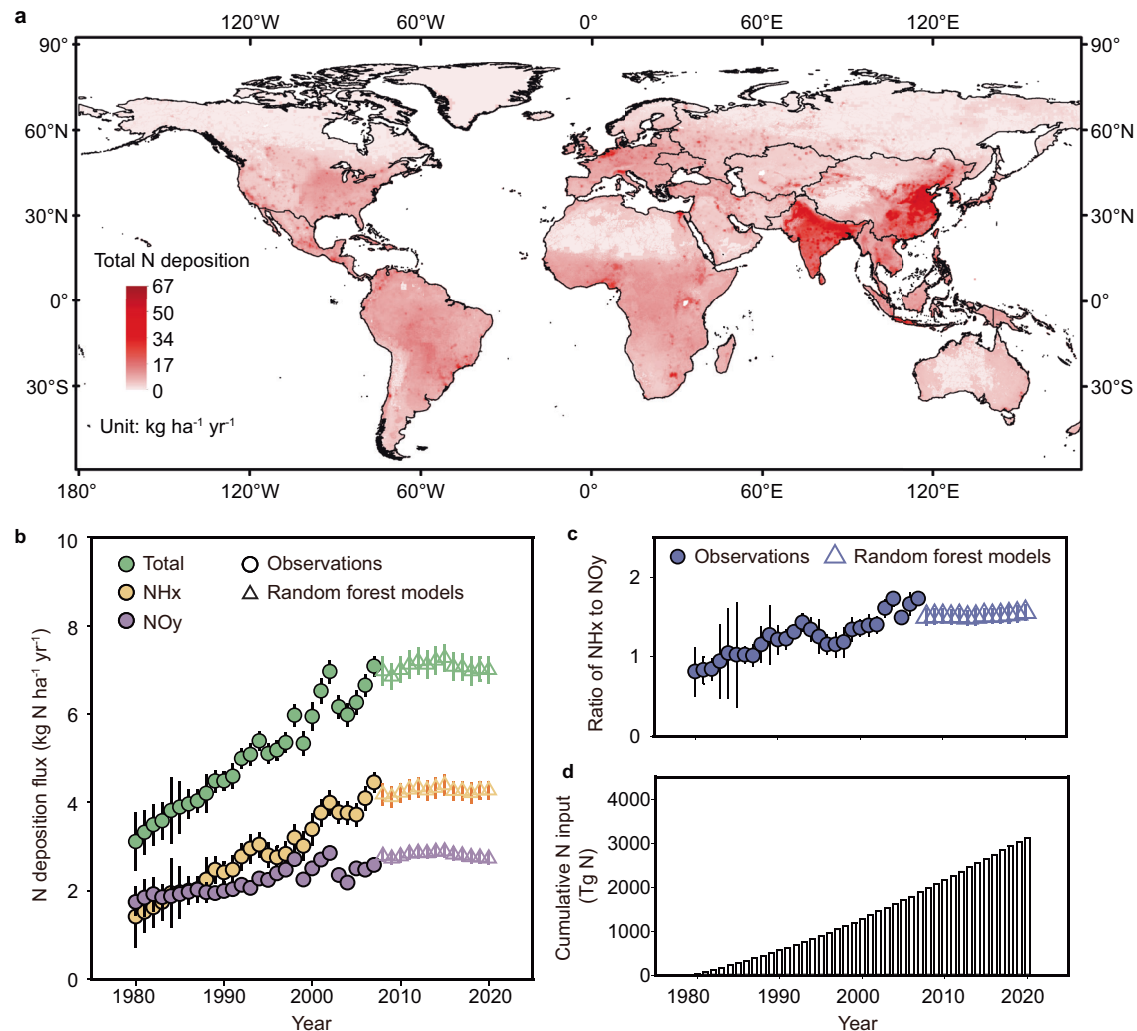**Fig. 1 | Spatio-temporal patterns of global terrestrial N deposition. a** Spatial distribution of total N deposition in 2020. **b** Temporal dynamics of total, NHx, and NOy deposition from 1980 to 2020; the circles are direct observations and their error bars indicate SE (the variation among the monitoring sites); the triangles are estimated from random forest models and their error bars indicate SE (variations across three random forest models). Different colors represent different N deposition components. **c** Temporal dynamics of ratio of NHx to NOy deposition from 1980 to 2020. **d** Cumulative N deposition input from 1980 to 2020. Note: The Antarctic is not included. Source data are provided as a Source Data file.

Changes in global N deposition from 1980 to 2020

Global terrestrial F_{Tot} increased and then stabilized and slightly decreased during 1980–2020, reaching a peak in 2015 at 7.3 kg N ha^{-1} yr^{-1} (Fig. 1b). From 1980 to 1982, F_{NHx} was slightly lower than F_{NOy}, but the subsequent increase in F_{NHx} was much faster than that of F_{NOy}. F_{NHx} and F_{NOy} decreased slightly after 2015 (Fig. 1b). Over the last 40 years the ratio of F_{NHx} to F_{NOy} ($R_{NHx/NOy}$) has gradually increased from 0.81 in 1980 to a maximum of 1.73 in 2007. It then began to decline and stabilized at 1.5 after 2010 (Fig. 1c). The cumulative input of F_N to global land from 1980 to 2020 was approximately 3117 Tg N (Fig. 1d) whereas global N fertilizer use was approximately 3549 Tg N[22]. Thus, N inputs to terrestrial ecosystems through atmospheric deposition were almost equivalent to those of fertilizer N over that period.

Regional N deposition dynamics from 1980 to 2020

The regional dynamics of N deposition from 1980 to 2020 can be divided into three types (Fig. 2). Type 1 shows a decline, which predominantly occurs in developed countries such as North America, Western Europe, Japan and South Korea (Fig. 2a–c). Except in North America, F_{Tot}, F_{NHx} and F_{NOy} all decreased; in North America $R_{NHx/NOy}$ increased or was approximately constant. Type 2 shows transition and mainly occurs in China, Russia, West Asia and other middle-income countries (grouped by income class according to the World Bank classification, gross national income per capita between $1146 and $14,005) (Fig. 2d–f). Here F_{Tot}, F_{NHx} and F_{NOy} all first increased and then stabilized or decreased. F_{Tot} reached a maximum and $R_{NHx/NOy}$ decreased, as in China, or was approximately constant. It should be noted that, in contrast to our expectations, we found that N deposition in Africa also showed an increase and then stabilized (Supplementary Fig. 4). Further analysis revealed that the C_{NO2} and $PM_{2.5}$ in Africa have both been decreasing (Supplementary Fig. 4), and GDPpc has experienced stagnant growth in the past decade (Supplementary Fig. 5). Although C_{NH3} has slightly increased, it has not changed the overall decline of F_N in Africa. Type 3 shows an increase and predominantly occurs in low-income countries (gross national income per capita less than $1145) such as South Asia, Southeast Asia and South America. Here F_{Tot}, F_{NHx}, and F_{NOy} showed significant increases, and $R_{NHx/NOy}$ also increased (Fig. 2g–i).

Transfer of global N deposition hotspots from 2008 to 2020

The global terrestrial F_{Tot} has been relatively stable over the last decade (Fig. 1b) but, as noted above, F_N in developed countries decreased, whereas it increased in developing countries in South Asia, Southeast Asia and South America (Fig. 2). Our calculations suggest that global hotspots of F_N are moving from developed to developing regions. To
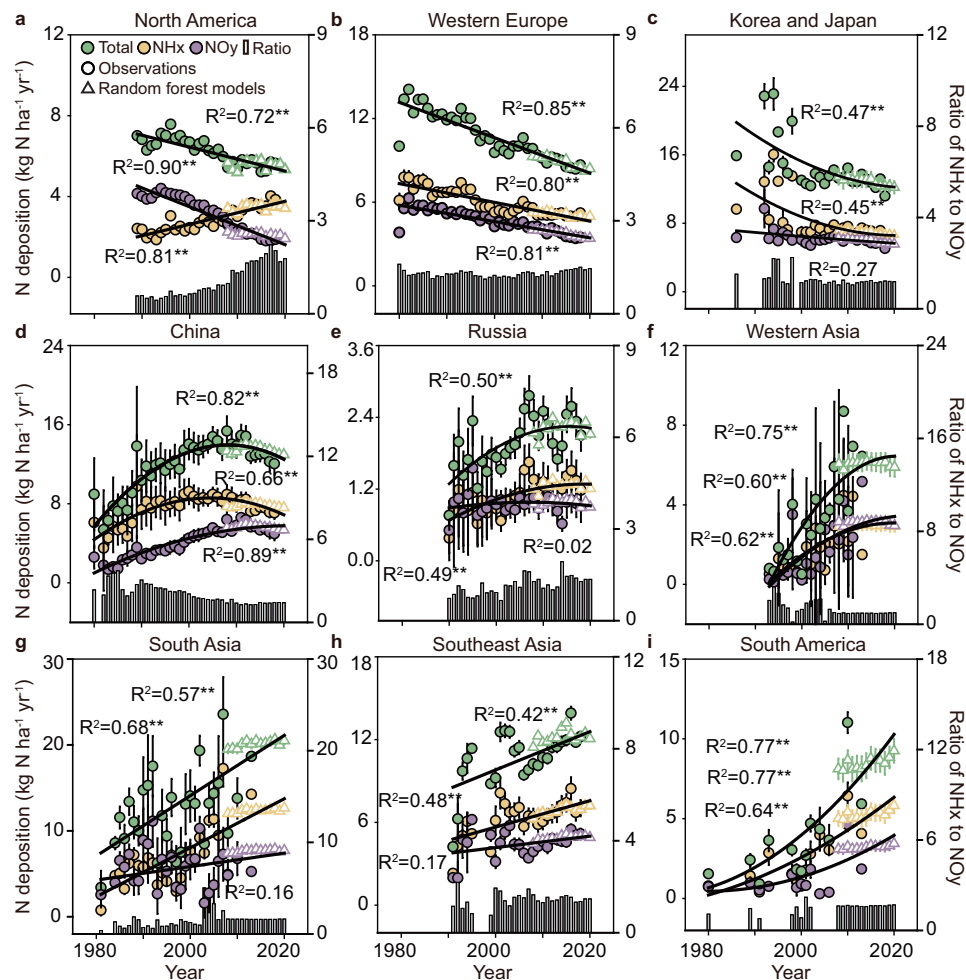
Fig. 2 | Regional dynamics of atmospheric N deposition from 1980 to 2020.
a Dynamics in North America. **b** Dynamics in Western Europe. **c** Dynamics in Korea and Japan. **d** Dynamics in China. **e** Dynamics in Russia. **f** Dynamics in Western Asia. **g** Dynamics in South Asia. **h** Dynamics in Southeast Asia. **i** Dynamics in South America. The circles are direct observations and their error bars indicate SE (the variation among the monitoring sites). The triangles are results from the random forest models and their error bars indicate SE (variations across three random forest models). Different colors represent different N deposition components. The trend of N deposition is fitted using linear or binomial functions. R^2 is the coefficient of determination, ** represents the significance level at $P = 0.01$, and * represents the significance level at $P = 0.05$. The bar chart at the bottom of each plot shows the dynamics of the ratio of NHx to NOy deposition in the region. Source data are provided as a Source Data file.

verify the robustness of this conclusion, we analyzed trends in F_{Tot} from 2008 to 2020. F_{Tot} significantly increased in developing countries at middle and low latitudes in South Asia, Southeast Asia, and Brazil. However, it significantly decreased in developed countries or regions such as Europe, the eastern United States, and Japan. Meanwhile, N deposition in some regions of Africa, West Asia, and Argentina has also decreased (Fig. 3a). Decreases of C_{NO2} and C_{NH3} in those regions of Africa, West Asia and Argentina could directly contribute to the decline of F_{Tot} in these areas (Supplementary fig. 6).

We also separately analyzed trends in F_N in developed and developing countries from 2008 to 2020. The dynamics of changes in F_N in developing and developed countries were different, with the ratio of F_{Tot} between developing and developed countries showing a significant linear increase ($R^2 = 0.43$, $P < 0.01$, Fig. 3b). In developed countries, the slight overall downtrend in F_N was primarily due to a significant decrease in F_{NOy} ($R^2 = 0.44$, $P < 0.05$), while F_{NHx} showed only a slight and non-significant decrease (Fig. 3c). This emphasizes the need for developed countries to strengthen measures to reduce NH_3 emission hotspots. In contrast, the significant increase in developing countries is due to the significant increase of F_{NHx} ($R^2 = 0.59$, $P < 0.01$, Fig. 3c).

We analyzed trends at sites with continuous observations of wet deposition data from 2000 (Supplementary Fig. 7). This confirms that

global hotspots of F_N have moved from developed to developing countries. It should be noted that these poorly monitored regions (i.e., Africa, Central Asia, Latin America, and Australia) still have the greatest uncertainty in F_N, and these highly uncertain regions include many of those with increasing trends, which requires further observation. Meanwhile, some long-term trends of indicators, such as foliar N content and surface water nitrate concentration, declined in United States[29–31] and Europe[32,33] and increased in tropical forest[34] and India[35], which potentially reflect the changing hotspots of F_N.

Drivers of global N deposition

E_{Nr} is an important mechanism driving the dynamic changes in F_N[15]. We analyzed the correlations between F_N and GDPpc, E_{Nr}, C_N and MAP in five major global regions at national and regional scales. E_{NH3}, NOx emissions (E_{NOx}), C_{NH3} and C_{NO2}, and MAP were correlated with F_{Tot}, F_{Wet} and F_{Dry}. The strength and positivity or negativity of the correlations varied according to region (Supplementary Fig. 8) showing that F_N is strongly influenced by anthropogenic E_{Nr} and meteorological factors, which is consistent with previous research[11,15].

Past research has developed a framework of active factors → E_{Nr} → meteorological factors → F_N to analyze the factors and mechanisms influencing F_N[3,26]. However, this does not clearly show the role of social
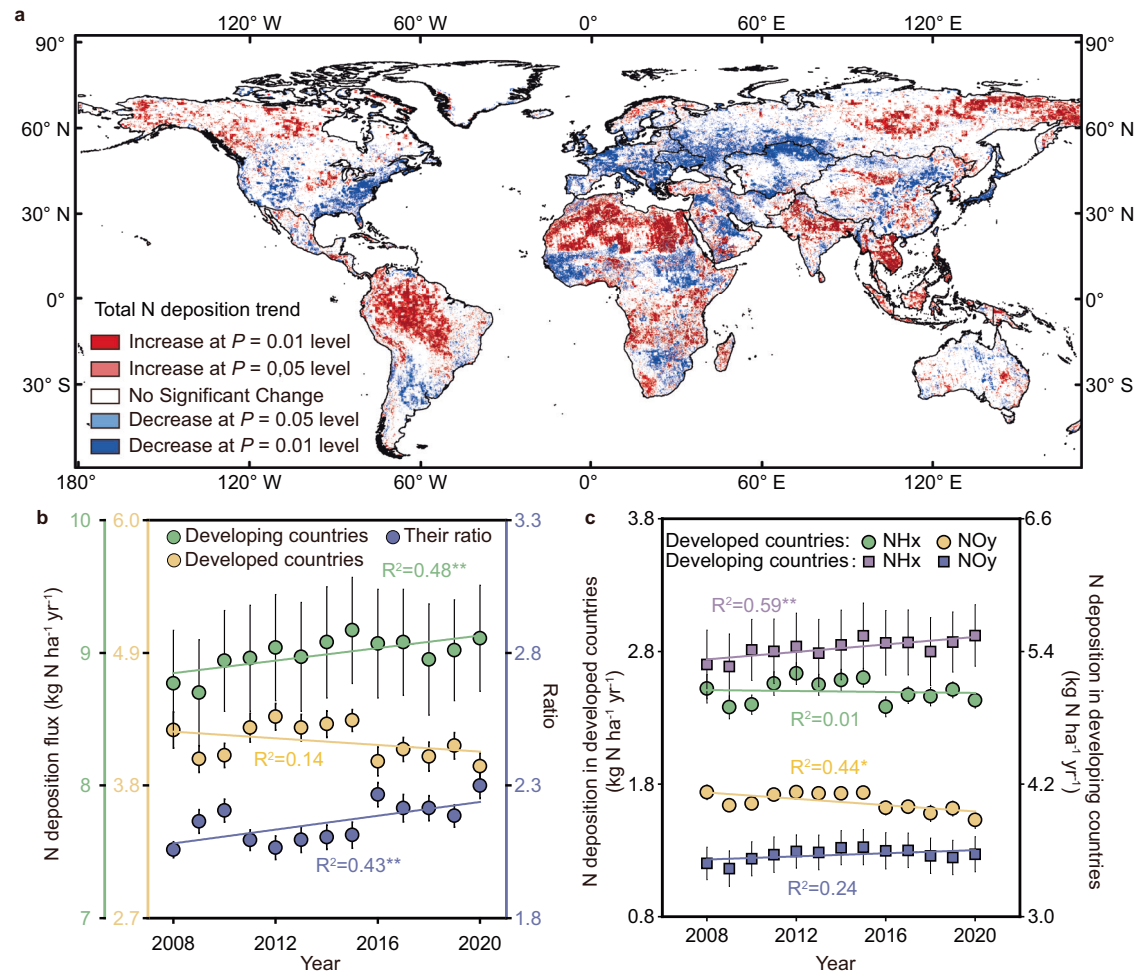
Fig. 3 | Trends in N deposition in developed and developing countries from 2008 to 2020. a Trend analysis of total N deposition from 2008 to 2020. **b** Temporal dynamics and ratios of total N deposition in developed and developing countries (Mean ± SE). **c** Temporal dynamics of NHx and NOy deposition in developed and developing countries (Mean ± SE). The trend of N deposition is fitted using linear or binomial functions. R^2 is the coefficient of determination, ** and * represents the significance level at $P = 0.01$ and $P = 0.05$, respectively, and SE (error bar in figure) indicated the variation across the three random forest models. Source data are provided as a Source Data file.

and economic development in changes in F_N. We found that GDPpc had a significant negative correlation with F_N in North America, Western Europe and East Asia. We also observed a less pronounced, less significant positive correlation with F_N in Southeast Asia and Africa (Supplementary Fig. 8). We therefore built a cascade network of GDPpc → E_{Nr} → C_N → MAP → F_N using structural equation models. The factors in these models and the processes that influence them can explain 45–88% of the spatiotemporal variation (Supplementary Figs. 9 and 10), confirming the importance of socioeconomic development in determining changes in F_N and its components.

We then analyzed the relationships between GDPpc and F_N at the global scale using data from several countries or regions. The relationships between F_{Tot}, F_{NHx}, F_{NOy}, F_{Wet}, F_{Dry} and GDPpc of countries or regions at different stages in their economic development fitted perfectly on a normal distribution curve (Fig. 4a–c; Supplementary Fig. 11a, b). This is consistent with the classical environmental Kuznets curve (EKC) model[19,36]. When we tested the logarithmic cubic equation model of EKC, the normal distribution curves were all significant ($P < 0.01$) (Fig. 4d–f; Supplementary Fig. 11c, d; Supplementary Table 3). The peak of F_{Tot} was at approximately \$8800, and the peaks of F_{Wet} and F_{Dry} were at \$8480 and \$8762 GDPpc (Supplementary Table 3), respectively. The peak for F_{NHx} was at approximately \$6600 and that of F_{NOy} at approximately \$11,000 GDPpc. F_{NHx} was predominantly derived from agricultural activities and reached its peak

before (in terms of time and/or economic development) F_{NOy}, which was mostly driven by industrial activities. This indicates that socioeconomic development, as expressed by GDPpc, is an important factor in determining the spatiotemporal pattern of F_N, and that the dynamic evolution of the relative contributions of agricultural and industrial activities determines the relationship between the peaks of F_{NHx} and F_{NOy}.

Implications for global N management

The cumulative input of F_N to terrestrial ecosystems from 1980 to 2020 (3117 Tg N) was almost equivalent to the global N fertilizer application (3549 Tg N) over the same period. N deposition can significantly increase the ecosystem productivity for forests, grasslands and water bodies[37,38], so the impact of such a substantial amount of natural N fertilization on the carbon cycle and carbon sink in ecosystems requires research[39], and the impacts of N deposition on species diversity, greenhouse gas emissions, soil acidification, etc., need to be re-assessed. Hotspots, areas of intensive N deposition, have moved from developed to developing countries at middle and low latitudes. Plant growth in tropical ecosystems in low latitudes is often limited by phosphorus[40], and an increase in N input tends to aggravate this limitation and reduce tree productivity[41], further threatening the structure and function of tropical ecosystems. Moreover, developed and developing countries have different dynamic trends of $R_{NHx/NOy}$

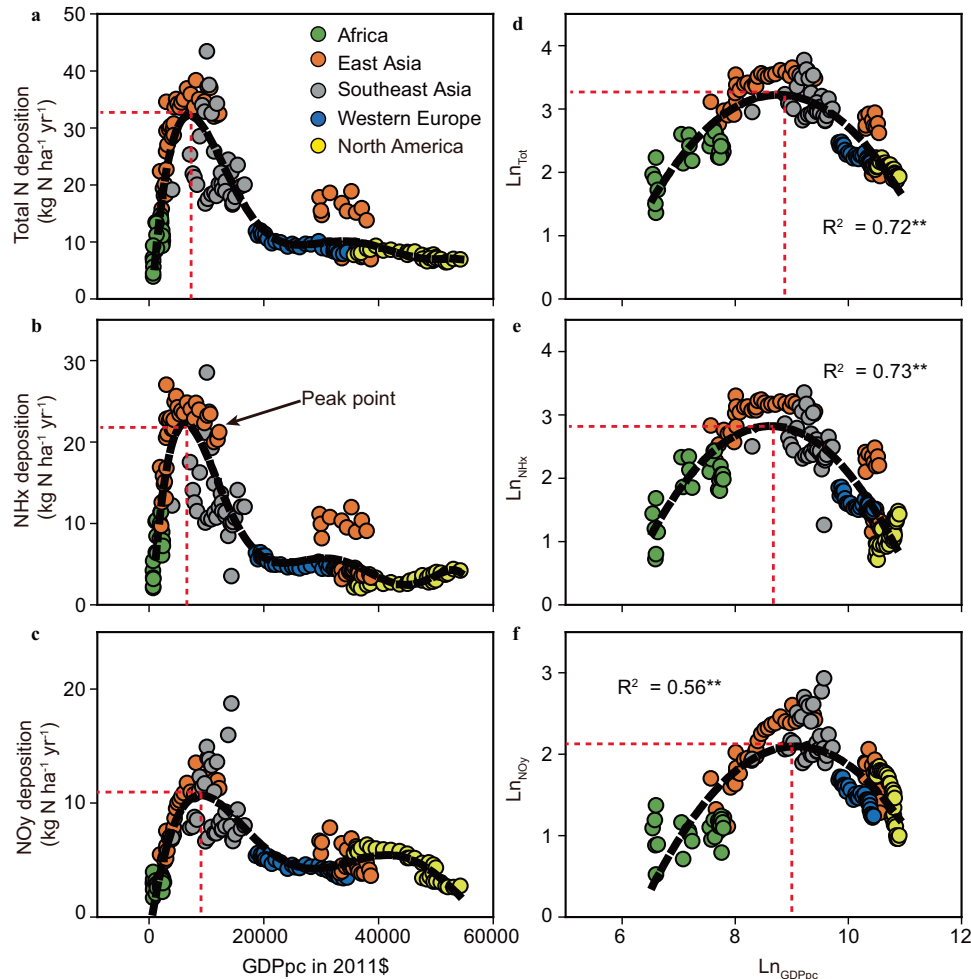**Fig. 4 | Relationships between N deposition and gross domestic product per capita on a global scale.** Relationships between total N (**a**, **d**), NHx (**b**, **e**) and NOy (**c**, **f**) deposition and gross domestic product per capita (GDPpc). The data used in **a**–**c** are observations of N deposition and GDPpc; those in **d**–**f** are the logarithmic values of N deposition and of GDPpc. African countries are Niger, Mali, Cameroon and Cote d'Ivoire. Southeast Asian countries are Vietnam, Malaysia, Indonesia and Thailand. East Asian countries are China, South Korea and Japan. Western European countries are EU countries (EU27). North American countries are the United States and Canada. R^2 is the coefficient of determination, ** represents the significance level at $P = 0.01$. Source data are provided as a Source Data file.

(Fig. 2), which affect ecosystems differently: plants can show a strong preference for NH_4^+ or NO_3^- [42,43] and the impacts of NH_4^+ and NO_3^- deposition on soil acidification and greenhouse gas emissions also differ[44,45]. Changes in $R_{NHx/NOy}$ may therefore lead to changes in the species composition of natural and semi-natural ecosystems.

Reducing N emissions and deposition in developing countries requires global cooperation and a better understanding of industry and agriculture contributions. F_{NHx} remained the dominant role in global N deposition in 2020, but the relative contribution of changing F_{NHx} to changes in F_N was decreasing (Supplementary Fig. 12). Meanwhile, we found that F_{NHx} from agriculture peaks before F_{NOy} mainly from industrial activities, with higher peak value for F_{NHx} (Fig. 4). The marginal cost of agricultural E_{NH3} reduction is substantially lower than industrial E_{NOx} reduction[46], making better N management in agriculture an economically efficient path for reducing N emissions while increasing crop yield and N use efficiency[47,48]. Thus, developing countries should prioritize agricultural emission reduction technologies to peak F_{NHx} before F_{NOy}. However, most countries lack clear NH_3 emission reduction policies and technologies[49]. Therefore, developing countries should fund agriculture to support rapid emission reduction technology applications alongside industrial development. By creating more efficient agriculture, developing and transitioning countries will avoid following the same path of N pollution as developed countries, and avoid the pollution events such as photochemical smog, acid rain, haze and soil acidification that Europe, North America and China have experienced[50,51].

Uncertainty analysis of global N deposition evaluation

Based on the MGND database, this study developed a framework to conduct a global grid dataset and systematically evaluate the current status, dynamic change, regional patterns, and hotspots transfers of global N deposition. This is a global evaluation independent of atmospheric chemical transport model simulations and based on extensive observation data. Although the estimated global total N deposition input to land (92.7 Tg N yr⁻¹) is higher than the results from atmospheric chemical transport model simulations (63.9–90.4 Tg N yr⁻¹)[23–25], by summarizing global natural and anthropogenic E_{Nr}, we found that total global E_{Nr} can reach -125.7–179.5 Tg N yr⁻¹ (Supplementary Table 2), indicating that our N deposition estimate is within a reasonable range.

Anthropogenic emission inventories (i.e., NH_3 and NOx) are important driving data for atmospheric chemical transport models that simulate atmospheric N deposition. Currently, inventories from the CEDS[28] and Emissions Database for Global Atmospheric Research (EDGAR)[52] are widely used in these models. These two datasets are estimated using a bottom-up approach based on emission activity information and emission factors. However, this approach is highly

uncertain, especially in regions lacking socio-economic statistics (such as Africa) and for NH_3 components whose emission factors are highly variable and more complex[53]. Recent studies using C_N to correct emission inventories have shown that bottom-up estimates of E_{Nr} are significantly underestimated, with E_{NOx} and E_{NH3} underestimated by about 22% and 38%, respectively (Supplementary Table 2)[53,54], which may contribute to the lower F_N estimates from models compared to our estimates.

We systematically compared the F_N estimates in North America, Europe and China from other studies with our study, as well as the corresponding E_{Nr}, and found consistent results across all studies (Supplementary Table 4). The relative uncertainty of F_N was less than 10% over most of areas (Supplementary Fig. 13). The uneven distribution of observation sites in the global atmospheric N deposition network may introduce bias in the machine learning models, especially in Africa, Central Asia, Latin America, and Australia, where sites are sparse. Although the cascading network of GDPpc $\rightarrow$ $E_{Nr} \rightarrow C_N \rightarrow$ meteorological factors$\rightarrow$ F_N is globally applicable, it is crucial to strengthen N deposition observations in regions with limited data to reduce evaluation uncertainty.

Methods
Collection of atmospheric N deposition site observation data
We used three sources of N deposition data: (1) data from 43 sites monitoring forests, grasslands, croplands, wetlands, deserts and cities from 2013 to 2020 in the Chinese Wet Deposition observation network (ChinaWD)[55]; (2) shared data from worldwide N deposition monitoring networks: European Monitoring and Evaluation Programme (EMEP) in Europe, the Clean Air Status and Trends Network (CASTNET), the Air Quality System (AQS), and the Ammonia Monitoring Network (AMoN) in the United States, the Canadian Air and Precipitation Monitoring Network (CAPMoN) and the National Air Pollution Surveillance Program (NAPS) in Canada, the Acid Deposition Monitoring Network (EANET) in East Asia, the International Network to Study Deposition and Atmospheric Composition in Africa (INDAAF), and the Nationwide Nitrogen Deposition Monitoring Network (NNDMN) from China Agricultural University[14]; (3) 1390 published papers reporting N deposition-related data from various locations (Supplementary Data 1). The criteria for selecting datasets from the literature were that the monitoring index had to include (i) ammonium, nitrate, total wet deposition (sum of ammonium and nitrate) or their concentrations in precipitation; (ii) the concentration or dry deposition of NH_3, NH_4^+, NO_2, HNO_3 and NO_3^-; (iii) daily, weekly or monthly observation frequencies; (iv) an observation period longer than one year.

The resultant MGND database includes site name, location, monitoring time, monitoring method, ecosystem type, annual rainfall, N concentration and flux of each component, and the data source. It spans 1977–2021 and includes 25,808 site years of wet deposition and 26,863 site years of dry deposition (Supplementary fig. 1 and Supplementary Table 1). Wet deposition comprised ammonium ($F_{Wet(NHx)}$) and nitrate ($F_{Wet(NOy)}$); dry deposition comprised gaseous NH_3 ($F_{Dry(NH3)}$), particulate NH_4^+ ($F_{Dry(NH4+)}$), gaseous NO_2 ($F_{Dry(NO2)}$), gaseous HNO_3 ($F_{Dry(HNO3)}$) and particulate NO_3^- ($F_{Dry(NO3-)}$) (Supplementary Table 1).

Sources of auxiliary analysis data
The sources of auxiliary analysis data and detailed information used in this study are shown in Supplementary Table 5. Meteorological data mainly come from Climatic Research Unit (CRU, version cru_ts4.05)[56] and the reanalysis product of NECP-NCAR (NECEP-NCAR Reanalysis 1)[57], including MAP, mean annual temperature (MAT), Wet days (WET), Vapor pressure (VAP), net shortwave radiation flux (Nswrs), surface pressure (Pres), specific humidity (Shum) and wind speed (Wspd).

Anthropogenic pollutants emission inventories were obtained from CEDS (version CEDS v_2021_04_21)[28]. We also used E_{NH3} from EDGAR 6.1[52] and Luo et al.[53]. C_{NH3} data were obtained from the Infrared Atmospheric Sounding Interferometer (IASI)[58]. We used the standard monthly scale reanalysis of tertiary data products for 2008–2020. C_{NO2} data were obtained from the Ozone Monitoring Instrument (OMI), Global Ozone Monitoring Experiment (GOME) and Scanning Imaging Absorption Spectrometer for Atmospheric Chartography (SCIAMACHY)[59]. The three satellite datasets were integrated into one dataset and covered 1996–2020[15]. SO_2 column concentration (C_{SO2}) were obtained from OMI/Aura SO_2 total column daily L3 data[60].

Data on the GDPpc and the population of each country were derived from the Maddison Project Database 2020[61]. The GDPpc were based on prices in 2011, which eliminated the impact of price changes and reflected the real values of product output over different periods. In addition, we also used $PM_{2.5}$[62], night light[63], grid GDP[64], population[65], Normalized Difference Vegetation Index (NDVI)[66], global production-living-ecological space data[67], terrestrial human footprint dataset[68], crop-specific N fertilization dataset[69], and statistics data on N fertilizer application per unit area[22] (Supplementary Table 5).

Analysis of temporal dynamic from site observation
We analyzed the variation of F_N in ten major countries or regions: Western Europe, North America, South America, Russia, Africa, Southeast Asia, South Asia, Western Asia, China, Japan and South Korea. The annual F_N in each area was calculated as the annual arithmetic mean and standard error of all the observed data for that area, including F_{NHx}, F_{NOy}, F_{Wet}, F_{Dry}, and F_{Tot}.

We used linear or nonlinear equations to analyze the trends in deposition from 1980 to 2020 in each area. We interpolated missing data based on the optimal fitted model for F_N with time for a specific area or period. Mean values and trends in global F_N were calculated using the weighted average method. We selected 352 observation sites with five years of continuous monitoring since 2000 and used the Mann–Kendall method to analyze F_{Wet} trends at the site scale.

All data were analyzed with SPSS version 13.0 statistical software. The correlations between F_N and GDPpc, E_{Nr}, C_N and MAP in five major global regions at national and regional scales were analyzed. The structural equation model was used to explore the predicators and influencing paths of F_N. All figures were drawn using SigmaPlot version 12.0 software. The spatial pattern figures for F_N were plotted with ArcGIS 10.0 software.

Construction of global N deposition grid dataset
We developed a framework to generate global grid F_N from site observation data between 2008 and 2020 (Supplementary Fig. 14). We did not extend the data to before 2008 due to insufficient data availability of some important variable (i.e., C_{NH3}). To minimize the influence of unevenly distribution observation sites on predicting global N deposition, we classified the global land into two categories: wilderness and human-modified area, based on global human footprint data, C_{NH3} and C_{NO2}. The global human footprint reflects various aspects of human pressures using eight variables, including built environments, population density, nighttime light, croplands, pasture lands, roadways, railways, and navigable waterways[68]. We defined wilderness areas as the intersection of regions where the global human footprint data is ≤1, C_{NH3} is in the lowest 10%, and C_{NO2} is in the lowest 2.5% for each year.

In general, wilderness areas are primarily located in high-latitude northern regions such as Alaska, Greenland, and Siberia, as well as the Sahara Desert in Africa, the Tibetan Plateau in China, and the desert regions of Australia. Our hypothesis is that these wilderness areas are less disturbed by anthropogenic activities, resulting in low levels of F_N. Areas with higher C_N have higher F_N. Therefore, F_N in these areas is

estimated as Eq. (1):

$$F_{N,i,j} = (Nor_{CNO2,j} + Nor_{CNH3,j}) \times 0.01 \tag{1}$$

where F_N represents the N deposition flux (kg N ha^{-1} yr^{-1}); Nor_{CNO2} represents normalization of C_{NO2}; Nor_{CNH3} represents normalization of C_{NH3}; i represents N components; j represents years from 2008 to 2020; 0.01 is a unit conversion factor that considers pre-industrial N deposition levels (kg N ha^{-1} yr^{-1}).

For human modified area, we used machine learning methods to upscale F_N from the site scale to the global grid scale. Only data from the main worldwide deposition observation networks was selected as the independent variable to achieve consistency and continuity of observations and methods. Notably, the random forest models demonstrated superior predictive accuracy, indicated by higher R^2 values both in the training and test sets, compared to support vector machine and BP neural network (Supplementary Table 6). We exclusively used random forest models to predict global N deposition in human-modified areas, employing three key pathways: the n6 model, the n22 best model, and the cascade model (Supplementary Table 7).

The randomForest package[70] in R software was used to build all the prediction model mentioned above. During model building, 70% of the data were randomly selected as the training set to evaluate the accuracy of the prediction model and 30% selected as the test set to evaluate the prediction performance of the model. The random forest models for F_{Dry} deposition were constructed using the ground monitoring concentrations of the different components. Deposition was estimated by multiplying the ground monitoring concentrations by the corresponding deposition velocity. We used recursive feature elimination (RFE) method to obtain the optimal variable combination in the n22 best model and the cascade model. Additionally, for all models, we used grid search method to select the best hyperparameters, such as the number of trees (between 100 and 1000), mtry (between 1 and the number of predictor variables or 1/3 of predictor variables for the n22 best models), and nodesize (the number of variables used at each node split, between 1 and the number of predictor variables), to maximize out-of-bag R^2 value. Shapley values (SHAP) were calculated to determine feature importance and analyze the sensitivity of the output to the input variable.

The n6 model was built with least variable combination based on the cascade network of GDPpc → E_{Nr} → C_N → MAP → F_N that was proven for China in our previous research[15]. The variation explained by the n6 models ranged from 72% to 83% (Supplementary Table 7). E_{Nr} was the most important predictor for most N deposition components while C_{NO2} was the most important predictors for ground HNO_3 and NO_3^- concentration (Supplementary Fig. 15).

The n22 best model builds on the n6 model, further enhancing its explanatory and predictive abilities. Using the RFE method, we optimized the best variable combination from 22 variables. As expected, the n22 best models' explanation rates are higher than those of the n6 models, except for ground HNO_3 and NO_3^- concentration (Supplementary Table 7). The most important predictor in the n22 best model was nearly the same as in the n6 models (Supplementary Fig. 16).

Given the large uncertainties in the emission inventory data, especially for E_{NH3}, we assumed this data would significantly impact the prediction results. Therefore, we designed the cascade model to first use C_N, economic activity, and land use to predict E_{NH3}. Then, we used the predicted NH_3 mission (pNH3), combined with C_N, meteorological factors, and atmospheric pollutant emission data, to predict F_N (Supplementary Table 7). We extracted four sets of raster data (E_{NH3} from CEDS, EDGAR, and two products in Luo et al.[53]) with less than 10% variation in E_{NH3}, identified as the more accurate raster data for E_{NH3} assessment, and used them as the dependent variable when predicting E_{NH3} in cascade model. C_{NH3} was the most important predictors for predicting E_{NH3}, and the variable pNH3 was the most important predictors for F_N (Supplementary Fig. 17).

Finally, we combined the N deposition dataset for wilderness and human-modified area to generate a spatial dataset for global F_N from 2008–2020 with a spatial resolution of 0.125° × 0.125°. The global annual input of N through deposition to land in 2020 was highest according to the cascade model (98.0 Tg N yr^{-1}), followed by the n22 best model (94.4 Tg N yr^{-1}), and then the n6 model (85.6 Tg N yr^{-1}) (Supplementary Table 8). The relative uncertainty at each pixel were calculated across three models. The relative uncertainty was defined as the ratio of standard error to the mean value of three models. We also used the Theil−Sen Median (Sen slope estimate) to analyze the trend of global N deposition during 2008–2020. The Mann−Kendall nonparametric test was used to determine the significance of the trends.

Relating deposition to economic growth

We integrated the global data of five regions – East Asia, Southeast Asia, Africa, Western Europe and North America – that had relatively long-term N deposition observations at different stages of social development into one reginal dataset. Two methods were used to analyze the relationship between F_N and GDPpc, and to determine whether it conforms to the EKC. Firstly, based on scatter plots, a high-order equation was used to explore the relationship between GDPpc and F_N in each area. Secondly, a logarithmic cubic equation (Eq. (2))[36] was used to analyze the relationship between F_N and GDPpc. The logarithmic cubic equation fitting parameters are listed in Supplementary Table 5.

$$\ln F_{Ni} = \alpha + \beta_1 * \left(\ln GDP_{pc} \right) + \beta_2 * \left(\ln GDP_{pc} \right)^2 + \beta_3 * \left(\ln GDP_{pc} \right)^3 \tag{2}$$

where GDP_{pc} is the real per capita GDP of each area in a certain year, F_N is the corresponding average N deposition flux, and i represents ammonium, nitrate, wet, dry or total deposition. β_0 is a constant and β_1, β_2, and β_3 are the estimated coefficients.

Reporting summary

Further information on research design is available in the Nature Portfolio Reporting Summary linked to this article.

Data availability

The global N deposition grid dataset (2008-2020) and source data are available at https://doi.org/10.6084/m9.figshare.26778574. Monitoring data from EANET are obtained from https://www.eanet.asia/. Monitoring data from EMEP are obtained from https://emep.int/. Monitoring data from CASTNET are obtained from https://www.epa.gov/castnet/download-data. Monitoring data from AQS are obtained from https://www.epa.gov/outdoor-air-quality-data. Monitoring data from AMoN are obtained from nadp.slh.wisc.edu/networks/ammonia-monitoring-network/. Monitoring data from CAPMoN are obtained from https://www.canada.ca/en/environment-climate-change/services/air-pollution/monitoring-networks-data.html. Monitoring data from APQMP are obtained from https://open.canada.ca/data/dataset/ed1d9a68-fce1-4dbc-8158-67d38019aef8. Source data are provided with this paper.

Code availability

The primary code used in this study is available at https://doi.org/10.6084/m9.figshare.26778574.

References

1. Malik, A. et al. Drivers of global nitrogen emissions. *Environ. Res. Lett.* **17**, 015006 (2022).
2. Fowler, D. et al. The global nitrogen cycle in the twenty-first century. *Philos. Trans. R. Soc. B* **368**, 20130164 (2013).
3. Dentener, F. et al. Nitrogen and sulfur deposition on regional and global scales: A multimodel evaluation. *Global Biogeochem. Cycles* **20**, GB4003 (2006).

4. Reay, D. S., Dentener, F., Smith, P., Grace, J. & Feely, R. A. Global nitrogen deposition and carbon sinks. *Nat. Geosci.* **1**, 430–437 (2008).

5. Thomas, R. Q., Canham, C. D., Weathers, K. C. & Goodale, C. L. Increased tree carbon storage in response to nitrogen deposition in the US. *Nat. Geosci.* **3**, 13–17 (2010).

6. Guo, J. H. et al. Significant acidification in major Chinese croplands. *Science* **327**, 1008–1010 (2010).

7. Bowman, W. D., Cleveland, C. C., Halada, L., Hresko, J. & Baron, J. S. Negative impact of nitrogen deposition on soil buffering capacity. *Nat. Geosci.* **1**, 767–770 (2008).

8. Bobbink, R. et al. Global assessment of nitrogen deposition effects on terrestrial plant diversity: a synthesis. *Ecol. Appl.* **20**, 30–59 (2010).

9. Richter, A., Burrows, J. P., Nuss, H., Granier, C. & Niemeier, U. Increase in tropospheric nitrogen dioxide over China observed from space. *Nature* **437**, 129–132 (2005).

10. Ge, Y., Vieno, M., Stevenson, D. S., Wind, P. & Heal, M. R. A new assessment of global and regional budgets, fluxes, and lifetimes of atmospheric reactive N and S gases and aerosols. *Atmos. Chem. Phys.* **22**, 8343–8368 (2022).

11. Liu, X. J. et al. Enhanced nitrogen deposition over China. *Nature* **494**, 459–462 (2013).

12. Engardt, M., Simpson, D., Schwikowski, M. & Granat, L. Deposition of sulphur and nitrogen in Europe 1900-2050. Model calculations and comparison to historical observations. *Tellus B: Chem. Phys. Meteorol.* **69**, 1328945 (2017).

13. Li, Y. et al. Increasing importance of deposition of reduced nitrogen in the United States. *Proc. Natl. Acad. Sci. USA.* **113**, 5874–5879 (2016).

14. Wen, Z. et al. Changes of nitrogen deposition in China from 1980 to 2018. *Environ. Int.* **144**, 106022 (2020).

15. Yu, G. et al. Stabilization of atmospheric nitrogen deposition in China over the past decade. *Nat. Geosci.* **12**, 424–429 (2019).

16. Uwizeye, A. et al. Nitrogen emissions along global livestock supply chains. *Nat. Food* **1**, 437–446 (2020).

17. Vet, R. et al. A global assessment of precipitation chemistry and deposition of sulfur, nitrogen, sea salt, base cations, organic acids, acidity and pH, and phosphorus. *Atmos. Environ.* **93**, 3–100 (2014).

18. Vishwakarma, S., Zhang, X., Dobermann, A., Heffer, P. & Zhou, F. Global nitrogen deposition inputs to cropland at national scale from 1961 to 2020. *Sci. Data* **10**, 488 (2023).

19. Gu, B. et al. Cleaning up nitrogen pollution may reduce future carbon sinks. *Global Environ. Change* **48**, 56–66 (2018).

20. Zhang, X. et al. Managing nitrogen for sustainable development. *Nature* **528**, 51–59 (2015).

21. UNEP. Launch of United Nations global campaign on sustainable nitrogen management, Colombo Declaration on Sustainable Nitrogen Management (accessed on 1 March 2020, available at https://papersmart.unon.org/resolution/sustainable-nitrogenmanagement). (2019).

22. FAO. FAOSTAT Fertilizers by Nutrient Database (accessed on 1 Jan 2022, available at https://www.fao.org/faostat/en/#data). (2021).

23. Tan, J. et al. Multi-model study of HTAP II on sulfur and nitrogen deposition. *Atmos. Chem. Phys.* **18**, 6847–6866 (2018).

24. Rubin, H. J. et al. Global nitrogen and sulfur deposition mapping using a measurement–model fusion approach. *Atmos. Chem. Phys.* **23**, 7091–7102 (2023).

25. Tian, H. et al. History of anthropogenic Nitrogen inputs (HaNi) to the terrestrial biosphere: a 5 arcmin resolution annual dataset from 1860 to 2019. *Earth Syst. Sci. Data* **14**, 4551–4568 (2022).

26. Ackerman, D., Millet, D. B. & Chen, X. Global estimates of inorganic nitrogen deposition across four decades. *Global Biogeochem. Cycles* **33**, 100–107 (2019).

27. Van Damme, M. et al. Global, regional and national trends of atmospheric ammonia derived from a decadal (2008-2018) satellite record. *Environ. Res. Lett.* **16**, 055017 (2021).

28. O'Rourke P. R. et al. CEDS v-2021_04_21 Gridded Emissions Data (accessed on 1 Dec 2021, available at https://data.pnnl.gov/dataset/CEDS-4-21-21). (2021).

29. Mason, R. E. et al. Evidence, causes, and consequences of declining nitrogen availability in terrestrial ecosystems. *Science* **376**, eabh3767 (2022).

30. McLauchlan, K. K., Ferguson, C. J., Wilson, I. E., Ocheltree, T. W. & Craine, J. M. Thirteen decades of foliar isotopes indicate declining nitrogen availability in central North American grasslands. *New Phytol.* **187**, 1135–1145 (2010).

31. Eshleman, K. N., Sabo, R. D. & Kline, K. M. Surface water quality is improving due to declining atmospheric N deposition. *Environ. Sci. Technol.* **47**, 12193–12200 (2013).

32. Penuelas, J. et al. Increasing atmospheric CO_2 concentrations correlate with declining nutritional status of European forests. *Commun. Biol.* **3**, 125 (2020).

33. Vuorenmaa, J. et al. Long-term changes (1990-2015) in the atmospheric deposition and runoff water chemistry of sulphate, inorganic nitrogen and acidity for forested catchments in Europe in relation to changes in emissions and hydrometeorological conditions. *Sci. Total Environ.* **625**, 1129–1145 (2018).

34. Hietz, P. et al. Long-term change in the nitrogen cycle of tropical forests. *Science* **334**, 664–666 (2011).

35. Pandey, J., Singh, A. V., Singh, A. & Singh, R. Impacts of changing atmospheric deposition chemistry on nitrogen and phosphorus loading to Ganga River (India). *Bull. Environ. Contamination Toxicol.* **91**, 184–190 (2013).

36. Dinda, S. Environmental Kuznets Curve hypothesis: A survey. *Ecol. Econ.* **49**, 431–455 (2004).

37. Eastman, B. A. et al. Altered plant carbon partitioning enhanced forest ecosystem carbon storage after 25 years of nitrogen additions. *New Phytol.* **230**, 1435–1448 (2021).

38. Stevens, C. J. et al. Anthropogenic nitrogen deposition predicts local grassland primary production worldwide. *Ecology* **96**, 1459–1465 (2015).

39. Zaehle, S. Terrestrial nitrogen - carbon cycle interactions at the global scale. *Philos. Trans. R. Soc. B* **368**, 20130125 (2013).

40. Du, E. Z. et al. Global patterns of terrestrial nitrogen and phosphorus limitation. *Nat. Geosci.* **13**, 221–226 (2020).

41. Li, Y., Niu, S. & Yu, G. Aggravated phosphorus limitation on biomass production under increasing nitrogen loading: a meta-analysis. *Global Change Biol.* **22**, 934–943 (2016).

42. Ashton, I. W., Miller, A. E., Bowman, W. D. & Suding, K. N. Niche complementarity due to plasticity in resource use: plant partitioning of chemical N forms. *Ecology* **91**, 3252–3260 (2010).

43. Song, M. H., Zheng, L. L., Suding, K. N., Yin, T. F. & Yu, F. H. Plasticity in nitrogen form uptake and preference in response to long-term nitrogen fertilization. *Plant Soil* **394**, 215–224 (2015).

44. Galloway, J. N. Acid deposition: Perspectives in time and space. *Water Air Soil Pollut.* **85**, 15–24 (1995).

45. Li, X. et al. The contrasting effects of deposited NH_4^+ and NO_3^- on soil CO_2, CH_4 and N_2O fluxes in a subtropical plantation, southern China. *Ecol. Eng.* **85**, 317–327 (2015).

46. Gu, B. J. et al. Abating ammonia is more cost-effective than nitrogen oxides for mitigating $PM_{2.5}$ air pollution. *Science* **374**, 758–762 (2021).

47. Gu, B. et al. Cost-effective mitigation of nitrogen pollution from global croplands. *Nature* **613**, 77–84 (2023).

48. Guo, Y. X. et al. Air quality, nitrogen use efficiency and food security in China are improved by cost-effective agricultural nitrogen management. *Nat. Food* **1**, 648–658 (2020).

49. Liu, L. et al. Exploring global changes in agricultural ammonia emissions and their contribution to nitrogen deposition since 1980. *Proc. Natl. Acad. Sci. USA.* **119**, e2121998119 (2022).

50. Fowler, D. et al. A chronology of global air quality. *Philos. Trans. R. Soc. A* **378**, 20190314 (2020).

51. Menz, F. C. & Seip, H. M. Acid rain in Europe and the United States: an update. *Environ. Sci. Policy* **7**, 253–265 (2004).

52. Johansson, L., Jalkanen, J.-P. & Kukkonen, J. Global assessment of shipping emissions in 2015 on a high spatial and temporal resolution. *Atmos. Environ.* **167**, 403–415 (2017).

53. Luo, Z. et al. Estimating global ammonia (NH_3) emissions based on IASI observations from 2008 to 2018. *Atmos. Chem. Phys.* **22**, 10375–10388 (2022).

54. Miyazaki, K. et al. Decadal changes in global surface NOx emissions from multi-constituent satellite data assimilation. *Atmos. Chem. Phys.* **17**, 807–837 (2017).

55. Zhu, J. et al. The composition, spatial patterns, and influencing factors of atmospheric wet nitrogen deposition in Chinese terrestrial ecosystems. *Sci. Total Environ.* **511**, 777–785 (2015).

56. Harris, I., Osborn, T. J., Jones, P. & Lister, D. Version 4 of the CRU TS monthly high-resolution gridded multivariate climate dataset. *Sci. Data* **7**, 109 (2020).

57. Kalnay, E. et al. The NCEP/NCAR 40-Year reanalysis project. *J. Bullet. Am. Meteorol. Soc.* **77**, 437–472 (1996).

58. Van Damme, M. et al. Version 2 of the IASI NH_3 neural network retrieval algorithm: near-real-time and reanalysed datasets. *Atmos. Meas. Tech.* **10**, 4905–4914 (2017).

59. Boersma, K. F. et al. An improved tropospheric NO_2 column retrieval algorithm for the Ozone Monitoring Instrument. *Atmos. Meas. Tech.* **4**, 1905–1928 (2011).

60. Li, C. et al. Version 2 Ozone Monitoring Instrument SO_2 product (OMSO2 V2): new anthropogenic SO_2 vertical column density dataset. *Atmos. Meas. Tech.* **13**, 6175–6191 (2020).

61. Bolt J., Jan LvZ. Maddison Project Database (accessed on 1 Feb 2022, available at https://www.rug.nl/ggdc/historicaldevelopment/maddison/releases/maddison-project-database-2020). (2020).

62. van Donkelaar, A. et al. Monthly global estimates of fine particulate matter and their uncertainty. *Environ. Sci. Technol.* **55**, 15287–15300 (2021).

63. Chen, Z. et al. An extended time series (2000–2018) of global NPP-VIIRS-like nighttime light data from a cross-sensor calibration. *Earth Syst. Sci. Data* **13**, 889–906 (2021).

64. Chen, J. et al. Global 1 km × 1 km gridded revised real gross domestic product and electricity consumption during 1992–2019 based on calibrated nighttime light data. *Sci. Data* **9**, 202 (2022).

65. K. Sims, et al. LandScan Global 2022 (access on 3 Agu 2022, available at https://doi.org/10.48690/1529167). (2022).

66. K. Didan, A. Huete, DAAC NL. MOD13C2 MODIS/Terra Vegetation Indices Monthly L3 Global 0.05Deg CMG (access on 5 Jun 2022, available at https://doi.org/10.5067/MODIS/MOD13C2.006). (2015).

67. Fu, J., Gao, Q., Jiang, D., Li, X. & Lin, G. Spatial–temporal distribution of global production–living–ecological space during the period 2000–2020. *Sci. Data* **10**, 589 (2023).

68. Mu, H. et al. A global record of annual terrestrial Human Footprint dataset from 2000 to 2018. *Sci. Data* **9**, 176 (2022).

69. Adalibieke, W., Cui, X., Cai, H., You, L. & Zhou, F. Global crop-specific nitrogen fertilization dataset in 1961–2020. *Sci. Data* **10**, 617 (2023).

70. Breiman, L. Random forests. *Mach. Learn.* **45**, 5–32 (2001).

Acknowledgements

Author contributions

G.Y. designed the research. J.Z., Y.J., N.H., Q.W., Z.C., H.H., X.Z., and P. L. conducted the research (collected the datasets and analyzed the data). J.Z., Y.J., and G.Y. wrote the manuscript. X.L., K.G., D.F., P.V. and F.Z. commented and revised on the manuscript.

Competing interests

The authors declare no competing interests.

Additional information

Supplementary information The online version contains supplementary material available at https://doi.org/10.1038/s41467-024-55606-y.

Correspondence and requests for materials should be addressed to Guirui Yu.

Peer review information *Nature Communications* thanks Hanqin Tian, and the other, anonymous, reviewer(s) for their contribution to the peer review of this work. A peer review file is available.

Reprints and permissions information is available at http://www.nature.com/reprints

Publisher's note Springer Nature remains neutral with regard to jurisdictional claims in published maps and institutional affiliations.